

**Giant dipole resonances and Coulomb correction effect  
in Delbrück scattering studied by elastic and Raman scattering  
of 8.5 to 11.4 MeV photons**

P. Rullhusen, U. Zurmühl, F. Smend, and M. Schumacher  
*II Physikalisches Institut, D3400 Göttingen, Federal Republic of Germany*

H. G. Börner and S. A. Kerr  
*Institut Max von Laue-Paul Langevin, F38042 Grenoble Cedex, France*  
(Received 25 August 1982)

Elastic and Raman scattering of 8.5 to 11.4 MeV  $\gamma$ -ray photons are investigated between charge numbers of 73 and 92. The experimental elastic scattering cross sections show large deviations from calculations based on available giant dipole resonance photoabsorption cross sections and on lowest order Delbrück amplitudes. The elastic differential cross sections measured at  $Z=83$  and 90 confirm the indications of a Coulomb correction effect in Delbrück scattering previously obtained for  $Z=92$  only. By a systematic analysis, quantitative information on the Coulomb correction effect in Delbrück scattering and on scaling factors for the giant dipole resonance photoabsorption cross sections is obtained.

[ NUCLEAR REACTIONS  $^{238}\text{U}$ ,  $^{232}\text{Th}$ ,  $^{209}\text{Bi}$  ( $\gamma, \gamma$ ), ( $\gamma, \gamma'$ ),  $E=8.5-11.4$   
MeV, measured  $\sigma(\theta)$ , elastic scattering, nuclear Raman scattering,  
Coulomb correction effect in Delbrück scattering. ]

## I. INTRODUCTION

Our present quantitative information on photoabsorption cross sections in the giant dipole resonance (GDR) region of heavy nuclei stems mainly from photoneutron experiments.<sup>1-3</sup> The data published by different laboratories for the same nucleus are in agreement with each other as far as the general shape of the GDR is concerned but differ by as much as 30% in the absolute photoabsorption cross sections. This uncertainty is of great importance, since it affects any information derived from the photoabsorption cross sections, e.g., (i) the extent to which the GDR exhausts the Thomas-Reiche-Kuhn (TRK) sum rule and (ii) the polarizability of the nucleus.

In addition to photoabsorption measurements, photon scattering experiments have been carried out. In the GDR region elastic photon scattering is a coherent superposition of Delbrück scattering and nuclear scattering, where the latter process may be split up into nuclear Thomson and nuclear Rayleigh scattering. Though in principle elastic photon scattering may be used as an independent method to improve our quantitative knowledge of the GDR, the complex nature of the scattering process requires a good understanding of all the different contributions. One main difficulty is caused by Delbrück scattering, which has been calculated in lowest order

only.<sup>4-6</sup> From investigations of Delbrück scattering at 2.754 MeV (Refs. 7-9) and 1 to 7 GeV (Ref. 10), it is well known that Coulomb corrections largely modify the Delbrück amplitudes. It would be surprising if Coulomb corrections were negligible in the GDR region of energies. The same conclusion may be drawn from the pair production cross section,<sup>11</sup> showing that Coulomb corrections are important at all energies.

Experimental indications of Coulomb corrections to Delbrück scattering at 9.0 MeV have been reported by the Negev Group.<sup>12</sup> However, a later reinvestigation<sup>13</sup> showed that the predicted elastic scattering cross sections used in the former work<sup>12</sup> were in error due to an incorrect sign in the tabulations of lowest-order Delbrück amplitudes.<sup>5</sup> In a recent reinvestigation<sup>9</sup> of elastic scattering at  $Z=92$  and  $E=9.0$  MeV we have shown that with the correct Delbrück amplitudes the indications for Coulomb corrections are retained.

The purpose of the present work was to confirm the Coulomb correction effect at 9.0 MeV and to obtain quantitative information on the Coulomb correction terms. For this purpose we have measured differential cross sections for elastic photon scattering in the 8.5 to 11.4 MeV energy region as a function of scattering angle and of charge number. One guide to the identification of the Coulomb correction effect is the strong evidence for the as-

sumption that Coulomb correction terms basically follow a  $Z^4$  dependence. This  $Z^4$  dependence has been unambiguously confirmed at 2.754 MeV.<sup>9</sup> Furthermore, the analysis of Fig. 7 in Ref. 10 shows that the Coulomb correction effect has essentially a  $Z^4$  charge number dependence at a photon energy of 1.92 GeV, although additional contributions from higher powers in  $Z$  have been reported.<sup>10</sup> Finally, Coulomb correction effects in pair production have proven to be basically proportional to  $Z^4$ .<sup>11</sup> All these findings support the assumption that, in the 8.5 to 11.4 MeV range of energies, the Coulomb correction terms should also be proportional to  $Z^4$ .

## II. EXPERIMENT

For the experiment, a sample consisting of 5.5 g of Cr and 4.5 g of Ni was inserted into the center of the tangential through channel of the Grenoble high flux reactor. The experimental setup is depicted in Fig. 1. Three Ge(Li) detectors with efficiencies between 10% and 20% relative to a 7.6 cm  $\times$  7.6 cm NaI(Tl) crystal at 1.332 MeV were positioned at scattering angles of  $\theta=60^\circ$ ,  $90^\circ$ , and  $120^\circ$ . The Ge(Li) detectors were surrounded by lead housings and, in addition, by tightly closed neutron shields. Since the  $\gamma$  energies were above the neutron thresholds of the scatterers, 22 cm of borated paraffin were placed in front of the Ge(Li) detectors in order to reduce the flux of fast neutrons at the detector position to a tolerable amount. Figures 2 and 3 show the spectra of photons scattered by Bi and Th, respectively, through a scattering angle of  $90^\circ$ . The duration of the runs was about 7 d.

The beam profiles were shaped by the internal collimators of the beam tube and by external collimators. By use of a small (3 mm  $\times$  3 mm) aperture collimator in front of a 5.1 cm  $\times$  5.1 cm NaI(Tl) detector, a precise scan of the beam was carried out.

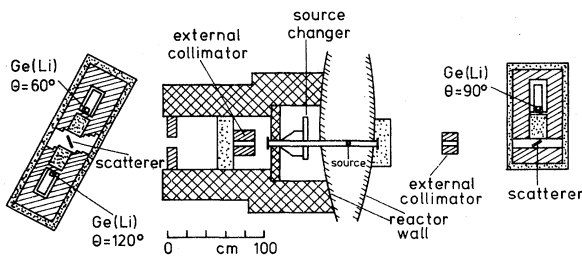


FIG. 1. Experimental arrangement. Hatched areas: lead shield. Dotted areas: borated paraffin or polyethylene with 0.4 cm  $B_4C$  sheets. Cross hatched areas: concrete walls. Distances between source and scatterers:  $r=13.0$  m ( $\theta=60^\circ$ ,  $120^\circ$ ) and  $r=7.8$  m ( $\theta=90^\circ$ ). Between the ends of the beam tube the drawing is not to scale.

With the same 3 mm  $\times$  3 mm aperture and a  $^{56}Co$  source the profile of the detection efficiency of each Ge(Li) detector was measured. This information served to properly evaluate the geometrical factor and the intensity of the direct beam. At the  $\theta=90^\circ$  position the beam profile was circular with a diameter of about 6 cm, whereas at the  $\theta=60^\circ$  and  $120^\circ$  positions the beam profile was rectangular with dimensions of 5 cm and 12 cm in the horizontal and vertical directions, respectively. In each of the geometries the dimensions of the scatterers were larger than the beam dimensions. The thicknesses of the scatterers were the following:  $^{238}U$ : 15.0 g/cm<sup>2</sup>;  $^{232}ThO_2$ : 4.37 g/cm<sup>2</sup>;  $^{209}Bi$ : 8.96 g/cm<sup>2</sup>; and  $^{nat}Pb$ : 13.5 g/cm<sup>2</sup>.

The experimental differential cross sections for elastic scattering are listed in Table I, and the experimental differential cross sections for Raman scattering are listed in Table II. All these data are new, except for the  $^{238}U$  elastic differential cross sections, which have been published in a previous paper.<sup>9</sup> The intensity of the 11.4 MeV  $\gamma$  line is different in the different primary  $\gamma$  spectra. This is due to the fact that this line stems from  $^{60}Ni$  formed by double neutron capture in  $^{58}Ni$  so that its intensity increases during the course of the experiments.

## III. THEORY

At energies well above the particle threshold the width of nuclear levels is in general much larger than the level spacing. Then the differential cross section is a smooth function of energy given by the coherent elastic differential cross section in the form

$$(d\sigma/d\Omega)^{coh} = \frac{1}{2} (|A_{||}|^2 + |A_{\perp}|^2), \quad (1)$$

where the scattering amplitudes are the sums of three terms

$$A = A^D + \tilde{A}^T + A^N, \quad (2)$$

i.e., for Delbrück ( $D$ ), nuclear Thomson ( $T$ ), and nuclear Rayleigh ( $N$ ) scattering. In Eq. (2) the classical Thomson formula is replaced by the modified version

$$\tilde{A}^T = -\frac{e^2}{Mc^2} g_{E1} \left\{ \left[ ZF_p(q) - \frac{NZ}{A} \right] + \kappa \frac{NZ}{A} [F_{ex}(q) - 1] \right\}, \quad (3)$$

which takes into account the form factors due to proton charges and exchange charges and has been previously discussed in more detail.<sup>9</sup> For the amplitudes  $A^N$ , the general expression

$$A^N = g_{E1} R^{E1}(E) + g_{E2} R^{E2}(E) \quad (4)$$

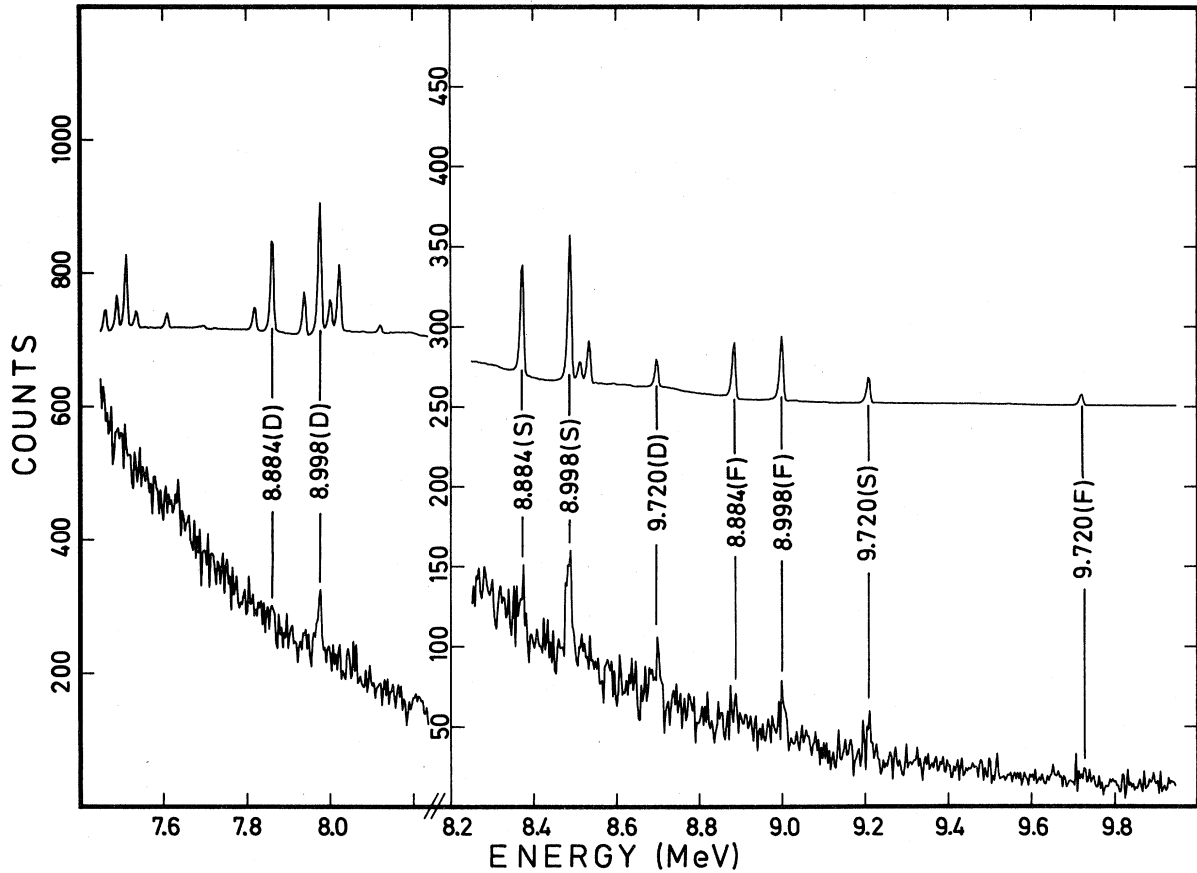


FIG. 2. Upper part: direct spectrum of photons emitted by the Ni-Cr neutron capture source. Lower part: spectrum of photons scattered by the  $^{209}\text{Bi}$  scatterer through  $\theta=90^\circ$ . *F*: full energy peak, *S*: single escape peak, *D*: double escape peak. The direct spectrum is not on scale.

is used, where the quantities  $R(E)$  represent the zero-angle amplitudes for scattering by the electric dipole and electric quadrupole giant resonances. The quantities  $g_{E_1, E_2}$  are the angular distribution coefficients.<sup>9</sup> Further details of the calculation of  $A^N$  have been described in a previous paper.<sup>9</sup>

In the discussion given above only the scalar part of the nuclear scattering which is coherent with the other scattering processes has been taken into account. For deformed nuclei, the tensorial excitation of the nucleus giving rise to incoherent elastic scattering for ground-state spins  $I_0 \geq 1$ , and to nuclear Raman scattering, must also be taken into account. In the modified simple rotator model (MSRM) (Ref. 14) the corresponding differential cross section is given by

$$(d\sigma/d\Omega)_i = (I_0 K_0 20 |I_f K_0|)^2 \times |2A_1 - A_2|^2 \frac{13 + \cos^2\theta}{40}. \quad (5)$$

In Eq. (5) the Clebsch-Gordan coefficient expresses the weight of the elastic incoherent part and of nu-

clear Raman scattering to the members of the ground-state rotational band of the scattering nucleus. The quantities  $A_j$  are the components of the elastic zero-angle scattering amplitude

$$R = \sum_{j=1}^2 A_j = \sum_{j=1}^2 \frac{\sigma_j \Gamma_j}{4\pi \hbar c} E^2 \frac{E_j^2 - E^2 + i\Gamma_j E}{(E_j^2 - E^2)^2 + \Gamma_j^2 E^2}, \quad (6)$$

where  $E_j$ ,  $\sigma_j$ , and  $\Gamma_j$  are the GDR parameters. The expression given in Eq. (5) implies that  $\sigma_2 \Gamma_2$  is larger than  $\sigma_1 \Gamma_1$  by a factor of the order of 2.

By comparing Eqs. (5) and (6) it can be seen that the two Lorentzian curves representing the GDR enter differently into elastic and Raman scattering. The elastic scattering measures the sum of the two constituents  $A_1$  and  $A_2$ , whereas Raman scattering depends on the difference. Therefore, provided the MSRM is the correct description of Raman scattering for rotational nuclei, two independent checks of the GDR parameters are obtained by observing elastic and Raman scattering.

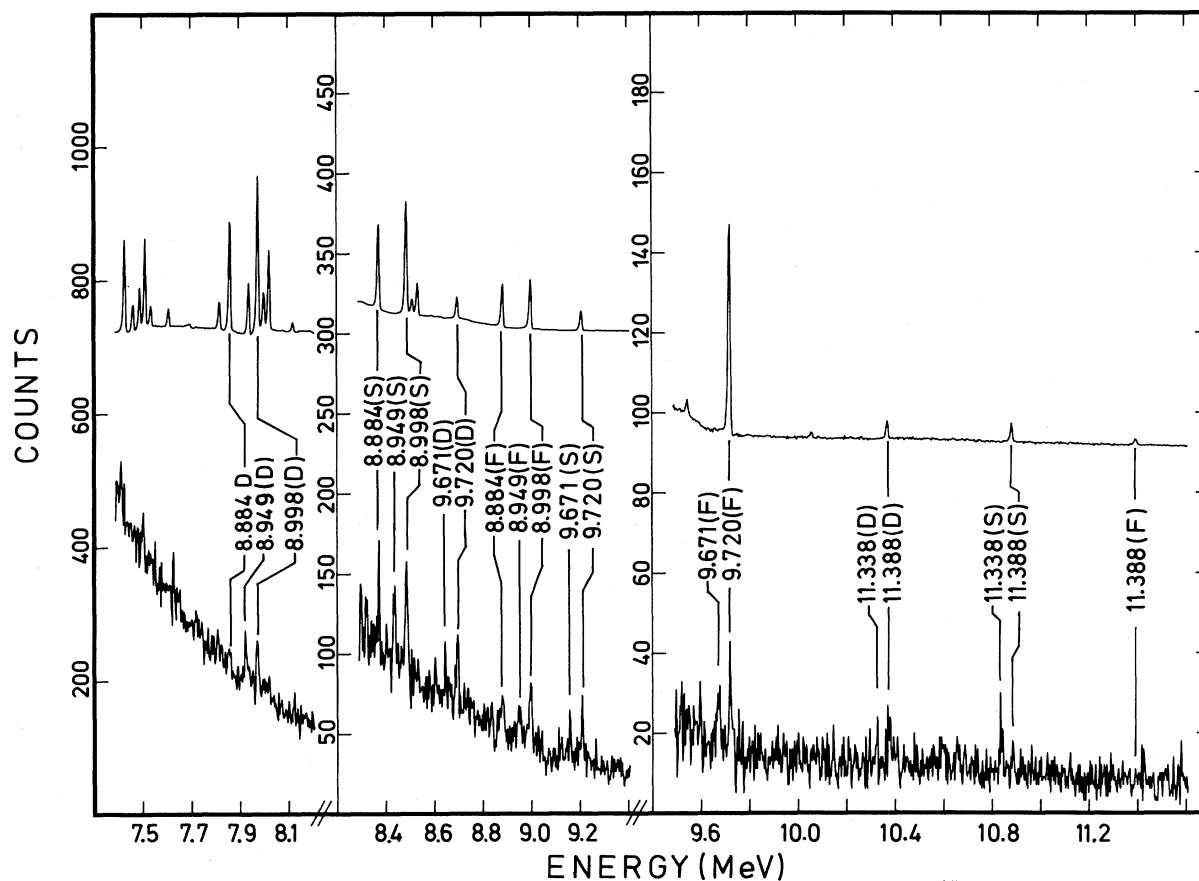


FIG. 3. Same as in Fig. 2 for the  $^{232}\text{Th}$  scatterer.

#### IV. DISCUSSION

Except for  $^{208}\text{Pb}$ , which has a fine structure,<sup>15-17</sup> the GDR of heavy nuclei seems to be well represented by one, or the superposition of two, Lorentzian curves fitted to the photoneutron cross sections. Deviations from these Lorentzian curves on the high energy side are due to the quasideuteron effect. There are also deviations on the low energy side for which no simple analytical representations can be given. A detailed discussion of the influence of the different effects on the amplitudes for nuclear

scattering in the 8.5 to 10 MeV energy range has been carried out in Table II and Fig. 7 of Ref. 9. The results may be summarized as follows. If one compares (i) a simple calculation based on the classical Thomson amplitude and  $E1$  resonance scattering as obtained from Lorentzian fits to the photoneutron cross sections with (ii) a more refined calculation taking into account the form factors due to proton charges and exchange charges, the  $E2$  resonances, the quasideuteron effect, and  $E1$  resonance scattering as obtained from the exact experimental photoabsorption data, differences of the order of

TABLE I. Differential cross sections for elastic scattering in  $\mu\text{b}/\text{sr}$ . Experimental errors are given in parentheses.

$E_\gamma$ (MeV)	$Z=92$		$Z=90$		$Z=83$		
	$\theta=90^\circ$	$\theta=60^\circ$	$\theta=90^\circ$	$\theta=120^\circ$	$\theta=60^\circ$	$\theta=120^\circ$	
8.533	17(9)		25.5(8.4)	7.7(5.9)		6.4(5.2)	3.7(2.6)
8.884	25(6)		21.4(4.6)	8.8(3.4)		8.4(2.5)	4.2(1.7)
8.998	30(3)	36(8)	22.1(4.0)	17.4(2.6)	29.0(4.3)	13.0(1.9)	9.6(1.3)
9.720	73(11)	61(23)	47.6(9.1)	42.9(8.6)	39(13)	23.7(4.8)	14.0(4.2)
11.388			219(86)		375(147)		189(47)

TABLE II. Differential cross sections for Raman scattering in  $\mu\text{b}/\text{sr}$ .

$E_\gamma$ (MeV)	$Z=92$		$Z=90$	
	$\theta=90^\circ$	$\theta=60^\circ$	$\theta=90^\circ$	$\theta=120^\circ$
8.884	21(6)		11.0(4.5)	9.1(3.8)
8.998	19(3)	19.2(6.1)	18.8(3.2)	8.8(2.4)
9.720	48(14)	28(22)	39.9(9.0)	28.5(8.4)
11.388			173(85)	

10% to 20% are obtained for the calculated differential cross sections at large angles. These differences are due, only to a minor extent, to the use of Lorentzian fits instead of the exact experimental photoabsorption data. Therefore, in view of the large differences in the predicted elastic differential cross sections obtained by applying GDR parameters from different experiments, the use of Lorentzian fits appears to be justified in the following discussion. Furthermore, the uncertainties caused by the form factors, the  $E2$  giant resonances, and the quasideuteron effect may be considered small.

Figures 4–6 show elastic differential cross sec-

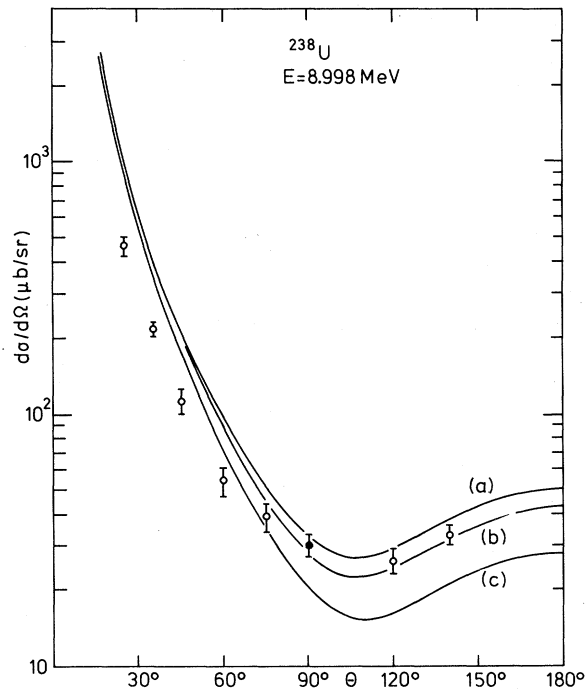


FIG. 4. Differential cross sections for elastic scattering of 8.998 MeV photons by  $^{238}\text{U}$ . Closed circles are from the present work, open circles are from Ref. 12. The predictions include  $N$ ,  $T$ , and lowest order  $D$  scattering with corrections for the form factors and GQR scattering. (a) calculated from the GDR parameters of Ref. 3; (b) same as (a) but GDR parameters  $\sigma_1$  and  $\sigma_2$  multiplied by 0.95; (c) calculated from GDR parameters of Ref. 2.

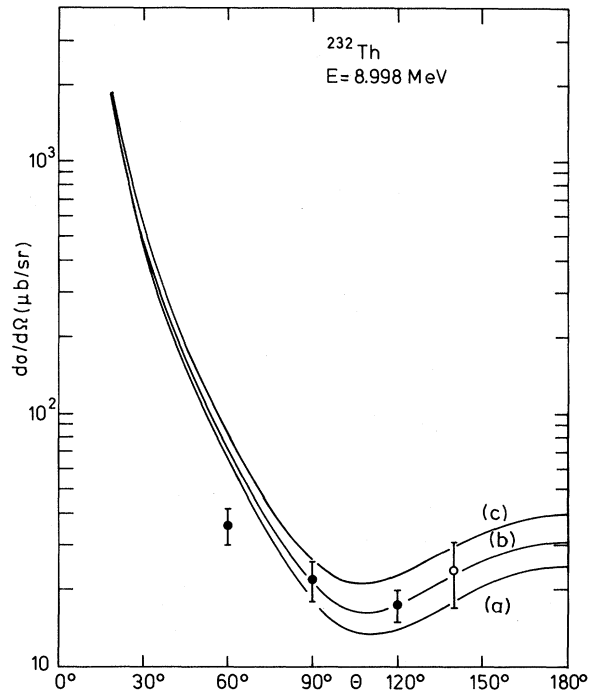


FIG. 5. Same as in Fig. 4 but for  $^{232}\text{Th}$ . Closed circles are from the present work, open circles are from Ref. 27. (a) calculated from GDR parameters of Ref. 2, (b) same as (a) but GDR parameters  $\sigma_1$  and  $\sigma_2$  multiplied by 1.25, (c) calculated from GDR parameters of Ref. 3.

tions for  $E=8.998$  MeV and the  $^{238}\text{U}$ ,  $^{232}\text{Th}$ , and  $^{209}\text{Bi}$  scattering targets. The experimental data are compared with calculations including the lowest-order  $D$ ,  $T$ , and  $N$  amplitudes with corrections for the proton and exchange-charge form factors and the giant quadrupole resonance (GQR). Curves (a) and (c) are obtained by using photoabsorption cross sections from different experiments. As mentioned before, there are sizable discrepancies between these predictions—up to a factor of 8 observed in the case of  $^{209}\text{Bi}$ . The large size of these discrepancies is caused by the destructive interference between  $T$  and  $N$  scattering, which makes the differential cross sections quite sensitive to the GDR parameters. Curves (b) have been obtained by applying a scaling factor to the photoabsorption cross sections used in the calculations of curves (a) in order to adjust theory to experiment at large scattering angles. These curves (b) show a systematic deviation from the experimental data at angles below  $90^\circ$  for all scattering targets, thus confirming the finding previously made for  $^{238}\text{U}$  only. In order to make quite sure that these discrepancies are due to Coulomb corrections in the  $D$  amplitudes, a procedure has been developed by which quantitative information

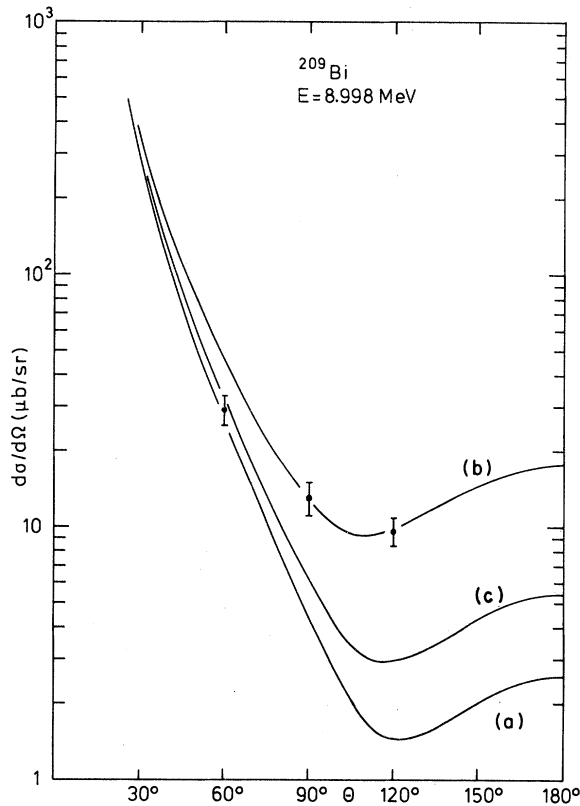


FIG. 6. Same as in Fig. 4 but for  $^{209}\text{Bi}$ . Experimental data from present work. (a) calculated from GDR parameters of Ref. 19, (b) same as (a) but GDR parameters  $\sigma_1$  and  $\sigma_2$  multiplied by 1.43, (c) calculated from GDR parameters of Ref. 20.

on the Coulomb correction terms was obtained and by which it was shown that the Coulomb correction terms are indeed in line with the  $Z^4$  charge number dependence discussed in the Introduction. This procedure is facilitated by the following facts:

(i) The number of four Coulomb correction amplitudes  $B^D$ , i.e.,  $\text{Re}B_{\parallel}^D$ ,  $\text{Re}B_{\perp}^D$ ,  $\text{Im}B_{\parallel}^D$ , and  $\text{Im}B_{\perp}^D$  may be reduced to one at large angles. From general arguments, the sum  $B_{\parallel}^D + B_{\perp}^D$  must be equal to zero at  $\theta = 180^\circ$ . Furthermore, it is observed that for both lowest-order amplitudes, i.e.,  $A_{\parallel}^D$  and  $A_{\perp}^D$ , real and imaginary parts are almost equal. Therefore, it is tentatively assumed the same holds for  $B_{\parallel}^D$  and  $B_{\perp}^D$ .

(ii) The  $N$  amplitudes rise dramatically when the photon energy is increased from 9.0 to 11.4 MeV, whereas the amplitudes for  $D$  scattering remain almost constant. Therefore, the elastic cross sections at 9.0 MeV are very sensitive to the  $D$  amplitudes, whereas the 11.4 MeV data are not. This allows the determination of improved GDR parameters mainly from the data at 11.4 MeV, and Coulomb correction

terms mainly from the data at 9.0 MeV. For the GDR, the possible number of free parameters was reduced to one by keeping the resonance energies  $E_j$  and widths  $\Gamma_j$  constant and by multiplying the cross sections  $\sigma_j$  by the same factor.

(iii) The remaining sensitivity of elastic differential cross sections to Coulomb corrections at 11.4 MeV is taken care of by observing that the well-known Coulomb correction terms at 2.754 MeV and the Coulomb correction terms introduced at 9.0 and 11.4 MeV are on a smooth curve.

Starting from these general considerations, functions of energy and scattering angle have been introduced in order to represent the Coulomb correction terms. By varying the scaling factor for  $\sigma_j$  and by trying to get good fits to all the available experimental cross sections between 2.754 and 11.4 MeV, it was possible to confine the scope of possible functions to a small group with very similar properties. During this procedure the following observations were made. At energies below 4 MeV the Coulomb correction terms  $B^D$  have to be of the same sign as the lowest-order amplitudes  $A^D$  in order to obtain agreement with experiment, whereas at energies above 7 MeV the signs must be opposite. In the intermediate energy region of 4–7 MeV Coulomb corrections apparently are of minor importance.<sup>13,21</sup> This observation is in line with the calculated<sup>11</sup> Coulomb correction terms of the pair production cross section which, for heavy elements, changes sign in the 5–6 MeV region. However, the energy dependence of the Coulomb correction terms in Delbrück scattering at large angles on one hand and pair production on the other hand are very different. As an example, Fig. 7 shows the energy dependence of Coulomb correction terms in Delbrück scattering

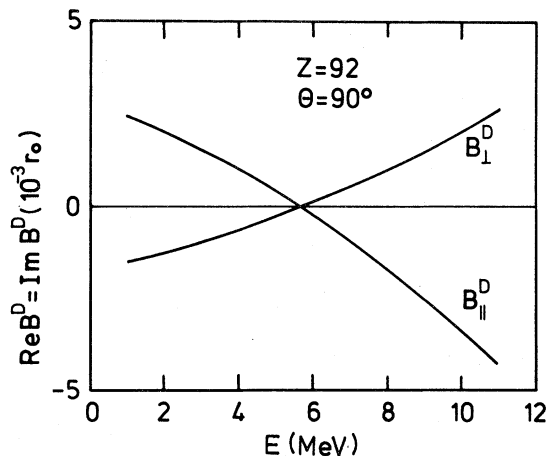


FIG. 7. Energy dependence of Coulomb correction terms for  $Z=92$  and  $\theta=90^\circ$ .

for  $Z=92$  and  $\theta=90^\circ$ .

In fitting empirical Coulomb correction terms  $B^D$  to the experimental data at  $Z=73, 83, 90,$  and  $92$  it was found that the amplitudes  $B^D$  are nearly independent of  $\theta$  for scattering angles  $\theta > 90^\circ$  but increase dramatically in magnitude for small scattering angles  $\theta < 45^\circ$ . The amplitudes  $B_1^D$  are of opposite signs in the forward and backward directions. This means that the Coulomb correction terms  $B^D$  very closely resemble the lowest-order amplitudes  $A^D$ . As examples, Figs. 8 and 9 show the lowest-order Delbrück amplitudes<sup>4,5</sup> and the Coulomb correction terms as a function of scattering angle. For most of the scattering angles use was made of the assumption that  $\text{Re}B_{||}^D = \text{Im}B_{||}^D$  and  $\text{Re}B_{\perp}^D = \text{Im}B_{\perp}^D$ . Slight differences were introduced, only for very small angles, in order to obtain better fits to the small-angle elastic differential cross sections. It can be seen from Fig. 8 that Coulomb correction and lowest-order terms are almost of the same size at these large charge numbers.

Figure 10 shows the comparison between theory and experiment at 11.4 MeV. Curves (a) and (b) are the final predictions including and not including the Coulomb correction terms, respectively. Curves (c) and (d) are obtained from curves (a) by varying the scaling factor of the photoabsorption cross sections by  $\pm 5\%$ . Within the experimental errors all four curves are consistent with the experimental data, with curves (a) giving the minimum  $\chi^2$ . This shows that the scaling factors of the photoabsorption cross sections are correct within about  $\pm 5\%$ , provided no major changes are necessary for the GDR parameters  $E_j$  and  $\Gamma_j$ . For a further improvement it would be very desirable to measure accurate elastic dif-

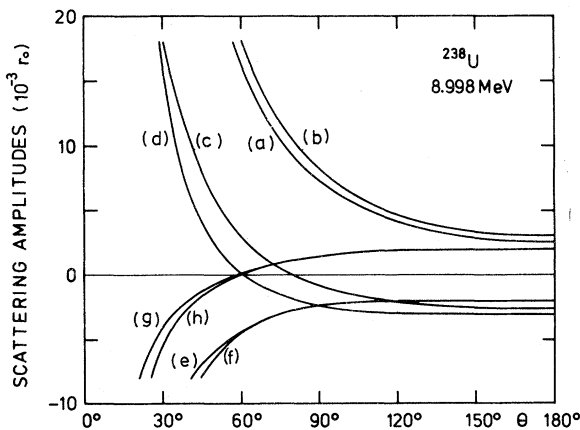


FIG. 8. Amplitudes for Delbrück scattering by  $^{238}\text{U}$ . Lowest-order amplitudes: (a)  $\text{Re}A_{||}^D$ , (b)  $\text{Im}A_{||}^D$ , (c)  $\text{Re}A_{\perp}^D$ , (d)  $\text{Im}A_{\perp}^D$ . Coulomb correction terms: (e)  $\text{Re}B_{||}^D$ , (f)  $\text{Im}B_{||}^D$ , (g)  $\text{Re}B_{\perp}^D$ , (h)  $\text{Im}B_{\perp}^D$ .

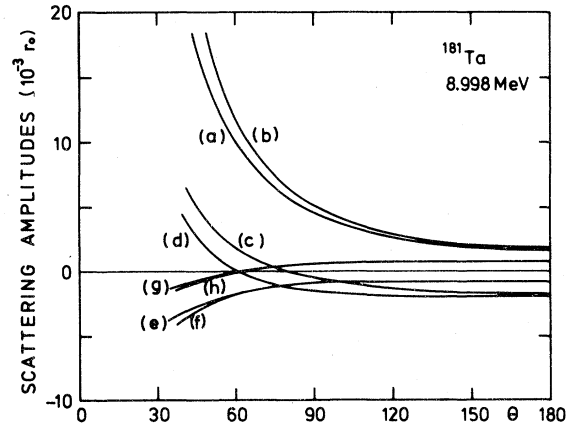


FIG. 9. Amplitudes for Delbrück scattering by  $^{181}\text{Ta}$ . Notation same as in Fig. 8.

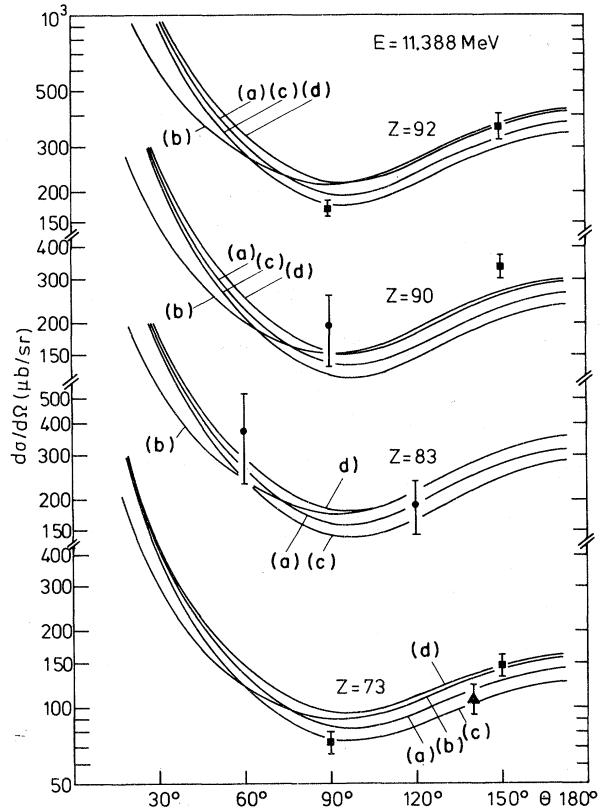


FIG. 10. Elastic differential cross sections for 11.4 MeV photons. Closed circles are from the present work, squares from Ref. 18, triangles from Ref. 22. (a) calculated including  $N$ ,  $T$ , lowest-order  $D$  amplitudes and Coulomb correction terms of  $D$  scattering. The GDR parameters are from the fitting procedure of the present work. Also included are the form factors and GQR scattering. (b) same as (a) but Coulomb correction terms omitted. (c) and (d) same as (a) but GDR parameters  $\sigma_1$  and  $\sigma_2$  varied by  $\pm 5\%$ .

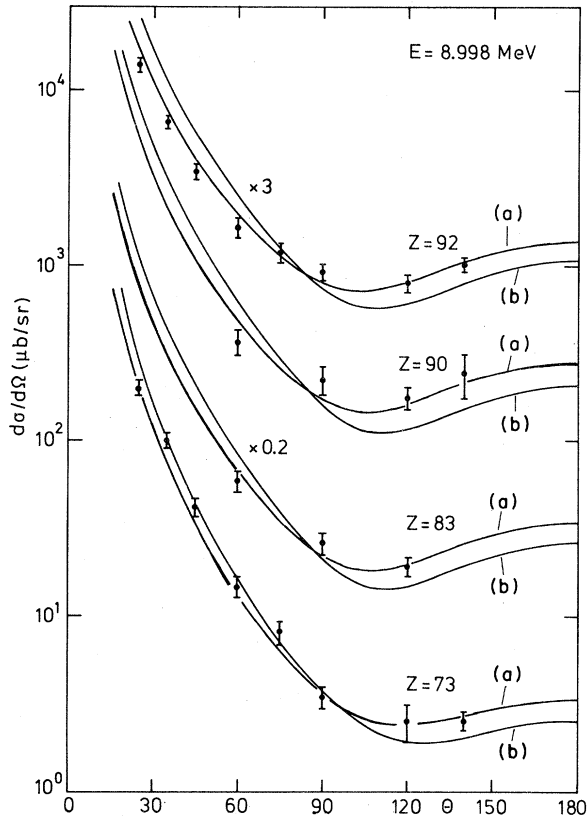


FIG. 11. Elastic differential cross sections for 9.0 MeV photons. For origin of experimental data for  $Z=92$ , 90, and 83 see Figs. 4–6; the experimental data for  $Z=73$  are from Ref. 23. Curves (a) and (b) have the same meaning as curves (a) and (b) in Fig. 10.

ferential cross sections over larger energy intervals. Figure 11 shows the comparison between theory and experiment at 9.0 MeV. Again curves (a) and (b) are the final predictions including and not including the Coulomb correction terms, respectively. Curves (a) are in satisfactory agreement with the experimental data for all scattering targets, whereas in Figs. 4–6 none of the curves had the appropriate shape. This gives clear evidence for the fact that elastic scattering at 9.0 MeV cannot be understood without including the Coulomb correction effect.

Figures 12 and 13 show a comparison between experimental and theoretical differential cross sections for Raman scattering. In Fig. 12 curves (a) and (b) have been calculated from the Saclay<sup>2</sup> GDR parameters with scaling factors of 1.00 and 1.06, respectively. Curves (c) and (d) were obtained from the Livermore<sup>3</sup> GDR parameters with scaling factors of 1.00 and 0.90, respectively. The two sets of parameters underlying curves (b) and (d) have led to the same good fit to the elastic scattering data, whereas for the Raman data, the fits of curves (c) and (d) are

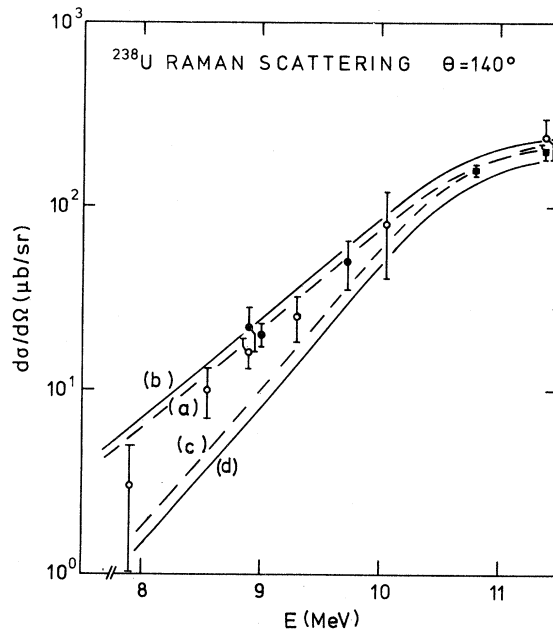


FIG. 12. Differential cross sections for Raman scattering by  $^{238}\text{U}$  through  $\theta=140^\circ$ . Closed circles are from the present work, transferred to  $\theta=140^\circ$ , open circles from Refs. 24, 26, and 27, squares from Ref. 18 and 25 transferred to  $\theta=140^\circ$ . (a) calculated from GDR parameters of Ref. 2, (b) same as (a) but GDR parameters  $\sigma_1$  and  $\sigma_2$  multiplied by 1.06, (c) calculated from GDR parameters of Ref. 3, (d) same as (c) but  $\sigma_1$  and  $\sigma_2$  multiplied by 0.90.

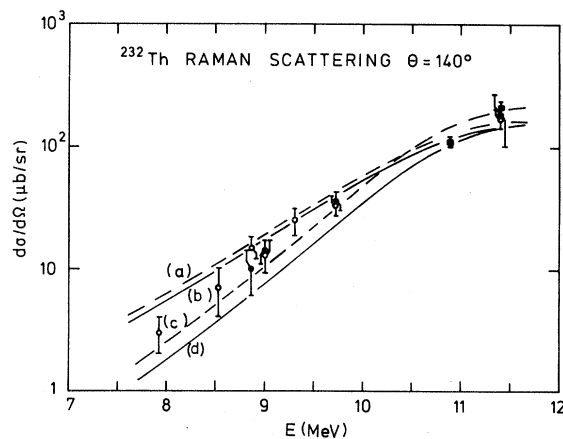


FIG. 13. Differential cross sections for Raman scattering by  $^{232}\text{Th}$  through  $\theta=140^\circ$ . Closed circles are from the present work, transferred to  $\theta=140^\circ$ , open circles from Refs. 26 and 27, squares from Refs. 18 and 25 transferred to  $\theta=140^\circ$ . (a) calculated from GDR parameters of Ref. 2, (b) same as (a) but GDR parameters  $\sigma_1$  and  $\sigma_2$  multiplied by 0.95, (c) calculated from GDR parameters of Ref. 3, (d) same as (c) but GDR parameters  $\sigma_1$  and  $\sigma_2$  multiplied by 0.85.

TABLE III. GDR parameters from previous photoneutron works and from present photon scattering work.

	$E_1$ (MeV)	$\sigma_1$ (mb)	$\Gamma_1$ (MeV)	$E_2$ (MeV)	$\sigma_2$ (mb)	$\Gamma_2$ (MeV)	Ref.
$^{238}\text{U}$	10.77	311	2.37	13.80	459	5.13	3
	10.96	301	2.90	14.04	369	4.53	2
	10.96	319	2.90	14.04	391	4.53	present work
$^{232}\text{Th}$	11.03	302	2.71	13.87	449	4.77	3
	11.08	268	3.37	14.07	349	4.62	2
	11.08	255	3.37	14.07	332	4.62	present work
$^{209}\text{Bi}$	13.56	648	3.72				20
	13.45	521	3.97				19
	13.45	703	3.97				present work

both inferior to the fits of curves (a) and (b). This means that as far as Raman scattering is concerned, the Saclay<sup>2</sup> parameters lead to a better agreement. Thus, the Saclay parameters with a scaling factor of 1.06 are the best choice for  $^{238}\text{U}$ . In Fig. 13 curves (a) and (b) have been calculated from the Saclay<sup>2</sup> GDR parameters with scaling factors of 1.00 and 0.95, respectively. Similarly, curves (c) and (d) are obtained from the Livermore<sup>3</sup> GDR parameters with scaling factors of 1.00 and 0.85, respectively. Again, the two sets of parameters underlying curves (b) and (d) have led to the same good fit to the elastic scattering data, whereas for Raman scattering the majority of the experimental data are slightly in favor of curve (b), i.e., the Saclay parameters with a scaling factor of 0.95. Table III contains the best-choice GDR parameters determined in the present work together with the original data. For  $^{209}\text{Bi}$  we have no arguments in favor of the one<sup>14</sup> or the other<sup>15</sup> set of GDR parameters. But, fortunately, in this case the two values given for  $E_1$  and  $\Gamma_1$  are very close to one another. For  $^{181}\text{Ta}$ , the GDR parameters already found by Bar-Noy and Moreh<sup>22</sup> have been confirmed.

## V. CONCLUSIONS

It has been shown that by a systematic study of the energy and charge-number dependence of elastic and Raman scattering quantitative information on the photoabsorption cross section and the Coulomb

correction effect in Delbrück scattering is obtained. The method of obtaining improved photoabsorption cross sections makes use of the observation that the main differences in the available GDR parameters are in the cross sections  $\sigma_i$ , whereas there is better agreement in the peak energies  $E_i$  and widths  $\Gamma_i$ . Furthermore, it was assumed (i) that  $\sigma_1$  and  $\sigma_2$  have to be modified by the same scaling factor and (ii) that Raman scattering is well described by the modified simple rotator model (MSRM). Irrespective of the fact that these assumptions are open to question, the best-choice GDR parameters obtained are a firm basis for the interpretation of Delbrück scattering in the 8.5 to 11.4 MeV energy range.

The information on the Coulomb correction effect relies on two assumptions: (i) Coulomb correction terms are basically proportional to  $Z^4$  and (ii) real and imaginary parts of the parallel and of the perpendicular amplitudes are almost equal in size in the 2.75 to 11.4 MeV energy range. Good arguments are presented in favor of both assumptions. Irrespective of the validity of these arguments it has become apparent that Coulomb correction terms of the same size as the lowest-order terms have to be introduced in order to reproduce the angular dependence of elastic differential cross sections observed at the charge numbers 83, 90, and 92.

The authors gratefully acknowledge the support of this work by the Deutsche Forschungsgemeinschaft.

- <sup>1</sup>B. L. Berman, *At. Data Nucl. Data Tables* **15**, 319 (1975).
- <sup>2</sup>A. Veyssi re, H. Beil, R. Berg re, P. Carlos, A. Lepr tre, and K. Kernbath, *Nucl. Phys.* **A199**, 45 (1973).
- <sup>3</sup>J. T. Caldwell, E. J. Dowdy, B. L. Berman, R. A. Alvarez, and P. Meyer, *Phys. Rev. C* **21**, 1215 (1980).
- <sup>4</sup>P. Papatzacos and K. Mork, *Phys. Rep.* **21C**, 81 (1975); *Phys. Rev. D* **12**, 206 (1975); and private communication.
- <sup>5</sup>T. Bar-Noy and S. Kahane, *Nucl. Phys.* **A288**, 132 (1977). Correct Delbr ck amplitudes are obtained by using  $A_{||} = M_{++} + M_{+-}$ ,  $A_{\perp} = M_{++} - M_{+-}$  instead of Eq. (6) and by changing the sign of  $\text{Im}M_{+-}$  in the heading of Table I. (All values in Table I are positive.)
- <sup>6</sup>P. Rullhusen, W. M ckenheim, F. Smend, M. Schumacher, G. P. A. Berg, K. Mork, and L. Kissel, *Phys. Rev. C* **23**, 1375 (1981).
- <sup>7</sup>P. Rullhusen, F. Smend, M. Schumacher, A. Hanser, and H. Rebel, *Z. Phys. A* **293**, 287 (1979).
- <sup>8</sup>M. Schumacher, F. Smend, P. Rullhusen, and W. M ckenheim, *Inst. Phys. Conf. Ser.* **62**, 598 (1982).
- <sup>9</sup>P. Rullhusen, U. Zurm hl, W. M ckenheim, F. Smend, M. Schumacher, and H. G. B rner, *Nucl. Phys.* **A382**, 79 (1982).
- <sup>10</sup>G. Jarlskog, L. J nsson, S. Pr nster, H. D. Schulz, H. J. Willutzki, and G. G. Winter, *Phys. Rev. D* **8**, 3813 (1973).
- <sup>11</sup>I. Øverb , K. J. Mork, and H. A. Olsen, *Phys. Rev. A* **8**, 668 (1973).
- <sup>12</sup>S. Kahane and R. Moreh, *Nucl. Phys.* **A308**, 88 (1978).
- <sup>13</sup>M. Schumacher, P. Rullhusen, F. Smend, W. M ckenheim, and H. G. B rner, *Nucl. Phys.* **A346**, 418 (1980).
- <sup>14</sup>T. Bar-Noy and R. Moreh, *Nucl. Phys.* **A275**, 151 (1977).
- <sup>15</sup>G. K hner, D. Meuer, S. M ller, A. Richter, E. Spamer, and O. Titze, *Phys. Lett.* **104B**, 189 (1981).
- <sup>16</sup>R. D. Starr, P. Axel, and L. S. Cardman, *Phys. Rev. C* **25**, 780 (1982).
- <sup>17</sup>Z. W. Bell, L. S. Cardman, and P. Axel, *Phys. Rev. C* **25**, 791 (1982).
- <sup>18</sup>H. E. Jackson, G. E. Thomas, and K. J. Wetzel, *Phys. Rev. C* **11**, 1664 (1975).
- <sup>19</sup>R. R. Harvey, J. T. Caldwell, R. L. Bramblett, and S. C. Fultz, *Phys. Rev.* **136**, B126 (1964).
- <sup>20</sup>L. M. Young, Ph.D. thesis, University of Illinois, 1972, (unpublished).
- <sup>21</sup>M. Schumacher, F. Smend, W. M ckenheim, P. Rullhusen, and H. G. B rner, *Z. Phys. A* **300**, 193 (1981).
- <sup>22</sup>T. Bar-Noy and R. Moreh, *Nucl. Phys.* **A288**, 192 (1977).
- <sup>23</sup>S. Kahane, T. Bar-Noy, and R. Moreh, *Nucl. Phys.* **A280**, 180 (1977).
- <sup>24</sup>T. Bar-Noy and R. Moreh, in *Photonuclear Reactions and Applications*, edited by B. L. Berman (U.S. AEC, Oak Ridge, Tennessee, 1973).
- <sup>25</sup>H. E. Jackson, G. E. Thomas, and K. J. Wetzel, *Phys. Rev. C* **9**, 1153 (1974).
- <sup>26</sup>T. Bar-Noy and R. Moreh, *Nucl. Phys.* **A229**, 417 (1974).
- <sup>27</sup>M. Hass, R. Moreh, and D. Salzmann, *Phys. Lett.* **36B**, 68 (1971).